Effect of the Wire Arc Additive Manufacturing Process Parameters on the Quality of Steel Components

By Anton A Kulikov, Maria V Grechneva & Andrei E Balanovskiy

Irkutsk National Research Technical University

Abstract- Wire arc additive manufacturing enables utilizing nearly any metallic alloy for the additive production of the geometrically complex parts and components of large scales. As an increasing number of materials are being used for WAAM, it is fundamental to conduct systematic research on the properties of various metals and alloys. This article presents a study of the influence of process parameters on the quality of the wire arc additively manufactured Sv-08G2S steel. During the experiments, the optimal process parameters were selected for the deposition of even and defect-free beads. The correlation between the process parameters and the bead geometry was determined. Adjustments of the parameters were made during the deposition of the walls consisting of a different number of layers. Once adjustments had been completed, more geometrically complex samples were manufactured. After deposition, the common defects and their possible causes were identified, and recommendations for their elimination were given. The obtained values of the ultimate tensile strength and yield strength of additively deposited steel are within the range and even exceed the characteristics of wrought low-carbon steels. Therefore, the conducted research has demonstrated that the wire arc additively manufactured Sv-08G2S steel provides the necessary quality and mechanical properties required for structural steels.

Keywords: additive manufacturing, wire arc additive manufacturing, gas metal arc welding, process parameters, steel, mechanical properties.

EFFECTOFTHEWIREARCADDITIVEMANUFACTURINGPROCESSPARAMETERSONTHEQUALITYOFSTEELCOMPONENTS

Strictly as per the compliance and regulations of:

Effect of the Wire Arc Additive Manufacturing Process Parameters on the Quality of Steel Components

Anton A Kulikov[α], Maria V Grechneva[σ] & Andrei E Balanovskiy[ρ]

Abstract- Wire arc additive manufacturing enables utilizing nearly any metallic alloy for the additive production of the geometrically complex parts and components of large scales. As an increasing number of materials are being used for WAAM, it is fundamental to conduct systematic research on the properties of various metals and alloys. This article presents a study of the influence of process parameters on the quality of the wire arc additively manufactured Sv-08G2S steel. During the experiments, the optimal process parameters were selected for the deposition of even and defect-free beads. The correlation between the process parameters and the bead geometry was determined. Adjustments of the parameters were made during the deposition of the walls consisting of a different number of layers. Once adjustments had been completed, more geometrically complex samples were manufactured. After deposition, the common defects and their possible causes were identified, and recommendations for their elimination were given. The obtained values of the ultimate tensile strength and yield strength of additively deposited steel are within the range and even exceed the characteristics of wrought low-carbon steels. Therefore, the conducted research has demonstrated that the wire arc additively manufactured Sv-08G2S steel provides the necessary quality and mechanical properties required for structural steels.

Keywords: additive manufacturing, wire arc additive manufacturing, gas metal arc welding, process parameters, steel, mechanical properties.

I. Introduction

The popularity of additive manufacturing (AM) and its rapid development are primarily related to the necessity of developing modern cost-effective manufacturing technologies. AM enables high-performance manufacturing of parts with complex geometric shapes. Another significant advantage of AM is a high material utilization rate combined with a low cost of feedstocks.

One of the latest technologies for 3D printing of metal products is wire arc additive manufacturing (WAAM). This technology combines industrial robots with off-the-shelf welding equipment. Thanks to the use of welding wires, the WAAM technology has a huge potential for printing almost any metal alloys [1-8]. Compared with the traditional subtractive manufacturing (machining), WAAM has a higher performance (40-60% higher), which helps to reduce the time of the finishing machining by 15-20%, depending on the size of the product [9].

The heat source is an electric arc generated between the substrate and the metal wire [10-13]. Welding wires are used as a feedstock material, which is much cheaper than metal powders used in other additive technologies [14-17]. Along with printing new parts, WAAM can also be used for repair and restoration operations [18].

The production of structurally strong, high-quality, reliable parts requires an understanding of the existing technological processes, underlying physical processes, raw materials, process control approaches, causes of various defects, and methods for their elimination. In order to produce parts with pre-set properties, it is instrumental to understand the principles of the microstructure evolution and mechanical properties of metals during the thermal impact.

As steels are still the most common industrial materials, they are of great interest to the WAAM community. On the one hand, the allotropy of iron-based alloys combined with high-temperature gradients makes it possible to produce components with a unique microstructure. On the other hand, alloys that may have different phase compositions depending on the cooling rate, such as martensite and retained austenite in steels with dispersion hardening will be sensitive to different thermal welding cycles. Therefore, steels require thorough research in order to be effectively applied in WAAM technology.

Due to the highly complex nature of metallurgical and welding processes occurring during deposition, many different aspects of the process need to be studied, including process development, process parameters, material quality and performance, the influence of heat input on characteristics of a final part.

This paper reviews the study of the effect of the various process parameters on the quality of the wire arc additively manufactured Sv-08G2S steel. The quality of the deposited steel was evaluated through micrographic analysis, Brinell hardness testing, and tensile testing.

Author α σ ρ: Irkutsk National Research Technical University, 83, Lermontov street, 664074 Irkutsk, Russian Federation.
e-mail: the.tosha2013@gmail.com

Year 2021

53

Global Journal of Researches in Engineering (J) Volume XXI Issue I Version I

© 2021 Global Journals

II. Methodology

The experimental robotic WAAM complex installed in the Irkutsk National Research Technical University was used to produce samples for this study and shown in Figure 1. The deposition of the wire was performed by the gas metal arc welding (GMAW) method using a KUKA KR 210 R2700 prime (KUKA robotics, Germany) with the Lorch SpeedPulse S3 mobil welding machine (Lorch, Germany).

Figure 1: Experimental robotic WAAM complex

The Sv-08G2S steel welding wire was used as a feedstock material. The chemical composition of this wire is presented in Table 1.

Table 1: Chemical composition of SV-08G2S wire

C	Si	Mn	Ni	S	P	Cr	N
0.06	0.8	1.9	0.2	0.02	0.02	0.1	0.01

Samples for microstructure analysis were cut across the central line of the deposited layers. Optical microscopy of the mechanically polished samples was performed in a cross-section. Samples were etched with Keller's reagent (2 ml HF, 3 ml HCl, and 5 ml HNO3 in 190 ml of water) to reveal the structure of the metal and grains. Electron microscopic studies were carried out on the basis of the Irkutsk National Research Technical University using a scanning electron microscope JIB-4501 JEOL multi-beam system equipped with an electronic and ion gun JIB-4501, completed with a nitrogen-free system of energy-dispersive microanalysis. The results were analyzed using the Channel 5 software package developed by Oxford Instruments. For these purposes, test samples had additionally passed the electro-polishing stage. The size of the scanning area for samples was 620 microns. The grain was taken as an area surrounded by large-angle borders, i.e. the value of the limit angle was set to 15°.

The microanalysis was followed by the Brinell hardness testing along the length of samples. The measurements present results of evaluating the hardness of sectors of samples from the first layer to the last. The HBRV – 187.5 hardness testing machine was used for measurements. Samples were used under a load of 7kH for 10 seconds. The HBRV – 187.5 hardness testing machine uses a rotational type of load change mechanism, as well as an optical measurement display system and a measuring microscope mounted on the device body. Polished (Ra < 0.04 microns) balls made of SHX15 steel with a nominal diameter of 5 mm were used as penetrators. The CDM-20 tensile testing machine was used for the tensile testing of samples.

III. Case Study

The parameters that have a major effect on the layer formation are found to be the torch travel speed, wire feed rate, and welding current. The selection of welding current was based on a wire diameter of 0.8 mm. The most suitable and optimal welding current for such diameter lies in the range of 100-120 A. Adjustment of these parameters allows achieving the desired quality of a deposited bead, its geometry, and the performance of the process Figure 2 illustrates five different beads produced at various deposition speeds.

Figure 2: Deposited beads using different process parameters

As can be seen from Table 2, the width of the bead varies depending on the torch travel speed. Bead №1 was deposited at a speed of 0.005 m/sec, which resulted in a too narrow bead with uneven melting of the metal. Applying this speed for the deposition of a real part, the accuracy of the geometric dimensions will be low, and the process of additive manufacturing as such will be unstable and difficult to control. Increasing the welding current while maintaining the same deposition speed did not give a positive result since it was necessary to increase the wire feed speed as well which led to the intensive scattering of the molten metal and the formation of an uneven geometry of the bead.

Table 2: Relationship between process parameters and the geometry of the deposited beads

Weld bead, №	Width, mm	Height, mm	Welding current, A	Welding Voltage, V	Wire feed rate, m/min	Torch travel speed, m/sec	Stickout distance, mm
1	4	2	100	26	4	0.005	14
2	6	3	120	28	5	0.004	13
3	8	3	120	28	4.5	0.003	11
4	10	2	120	28	4.5	0.002	11
5	12	2	120	28	4.5	0.001	11

When depositing bead №2, the deposition speed was reduced to 0.004 m/sec at a welding current of 120A. The reduction of the speed of deposition contributed to the formation of a bead of high quality since the metal was melted evenly with small distortions along the central axis. However, applying such deposition parameters, the height of the bead along the central line is significantly bigger than the height of the bead on the sides. It will negatively affect the formation of the next layers since the metal will not be able to evenly overlap the uneven surface of the previous layer. As a result, the metal will flow along the sides of the layer, leaving the centerline unfilled. In this case, it will be quite difficult to control the process and achieve the desired accuracy of the dimensions of real parts. Further reduction of the speed to 0.003 m/sec during the deposition of the bead №3 gave the most promising result.

The formation of the bead №3 is satisfactory enough; the layer itself is straight having the least distortion. The height of the bead is optimal and will contribute to the qualitative deposition of subsequent layers. Utilizing these parameters, it will be possible to predict the behavior of the metal during the deposition process and achieve dimensional accuracy.

The subsequent reduction of the speed to 0.002 and 0.001 m/sec during the deposition of samples №4 and №5 resulted in the production of the widest beads. Excessive heat input at these speeds leads to overheating of the metal and the formation of an inhomogeneous structure, which will inevitably contribute to the formation of defects. Additionally, applying such parameters, it will be quite difficult to achieve the dimension accuracy and quality of the deposited surface.

Ultimately, a linear relationship between the print speed (torch travel speed) and the width of the deposited bead was determined during the experiments (see Figure 3).
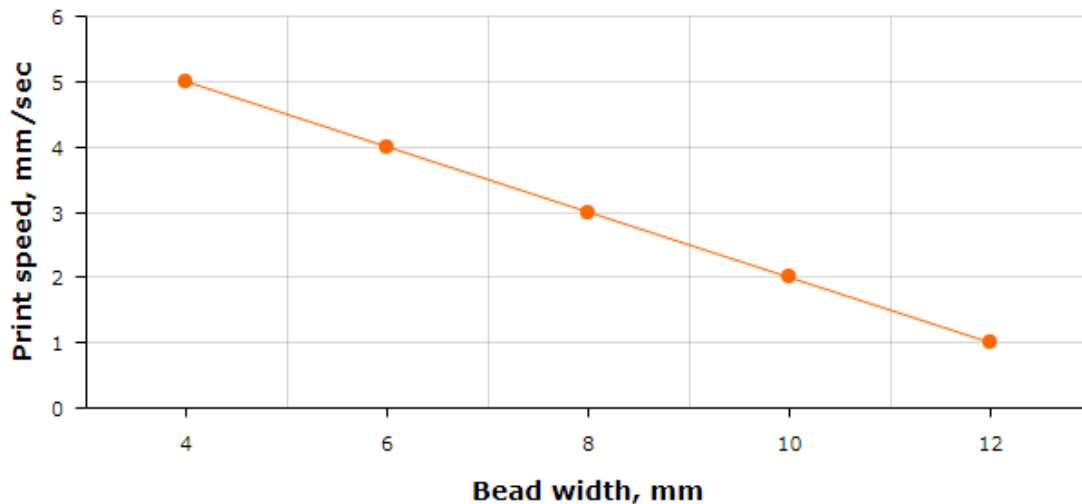

Figure 3: Correlation between print speed and bead width

Thus, the most optimal parameters for the deposition during this experiment are the following: welding current – 100 A, welding voltage – 26 V, wire feed rate – 4,5 m/min, torch travel speed – 0,003 m/sec, stick out distance – 11 mm). For the deposition of multi-layer samples, a more precise parameter setting will be required during the layering process, depending on the geometry of the resulting part. Figure 4 illustrates the multi-layer walls deposited using the above-mentioned parameters. Table 3 illustrates the obtained geometry of the walls.

Figure 4: Deposited walls

Table 3: Characteristics of the deposited walls

Wall, №	Number of layers	Height, mm	Length, mm	Wall thickness, mm	Welding current, A	Welding Voltage, V	Wire feed rate, m/min	Torch travel speed, m/sec	Stickout distance, mm
1	13	27	100	8	100	26	4.5	0.003	11
2	10	20	100	9	100	26	4.5	0.003	11
3	10	20	100	9	100	26	4.5	0.003	11

As can be seen from Table 3, the average thickness of one layer was 2 mm. The deposition speed of 0.003 m/sec is truly applicable for the deposition of even and fairly accurate layers, but the defects are still present. The most noticeable defects are the spreading of the metal and the slope of the wall at the end of the layer, which was the result of constant and severe heat input during the deposition process (see Figure 5).

Figure 5: Slope at the end of the wall

Furthermore, there are elements of non-molten wire and splashes of metal. Some layers are deposited with a slight offset relative to the central axis of the wall, which leads to uneven overall wall thickness. To obtain a more accurate geometry and reduce defects, it is necessary to control the heat input and constantly adjust the parameters during the deposition process.

During the course of the further experiment, a box with dimensions of 60x60 mm was deposited, the number of layers is 15, and the total height is 30 mm (see Figure 6). The average value of the layer thickness of 2 mm, determined in previous experiments, is also preserved during the deposition of a sample with a more complex geometric shape.

Figure 6: Deposited box

Layers' deposition in a square-shaped sample differs from that in the wall due to the presence of angles and the constant change of the movement trajectory of the welding torch. Since the torch was moving along a trajectory consisting of 4 linear movements, there were minor stoppages of the torch in the corners of the square. This has led to a slight widening of the beads at the corners, but this is not an issue since post-process machining will help to correct the situation. Essentially, the formation of a square-shaped part is quite successful, the deviation from the specified dimensions are within the allowance for machining, which indicates the potential of WAAM technology for production parts of the complex angular shape.

Then, the cylindrical samples were deposited (see Figure 7). Cylinder №1 has a diameter of 80 mm and consists of 11 layers with an overall height of 22 mm. Cylinder №2 has a diameter of 50 mm and consists of 24 layers with an overall height of 48 mm.

Figure 7: Deposited cylinders

The previously defined layer height of 2 mm remains unchanged during the deposition of cylindrical shaped samples. A cylinder with a larger diameter has a more even bead shape and has less distortion over the entire length of the layer in comparison with a cylinder with a smaller diameter. A special effect on the process of forming the cylinder has the choice of the point where the deposition of the next layer should starts. Since the deposition of each subsequent layer began at one point, a small roll was formed at this very place, which led to an uneven height of the cylinder and a broadening of the wall at this point. In order to eliminate this defect, it is necessary to change the start point of the deposition of each subsequent layer or to reduce the dwell time of the welding torch right before the deposition of the next layer.

The next step was to test the selected process parameters for printing more complex parts. The square-to-cylinder body is presented in Figure 8. The first layers of the body are box-shaped. Then, with each successive layer, the robot smoothed out the corners and switched to a cylindrical trajectory. The diameter of the cylinder was also constantly changing. A spiral motion algorithm was set for the torch movement. Such an approach made it possible to avoid stoppings of the torch when switching to a new layer and to increase the

performance of the deposition process since the robot carried out the whole trajectory in one movement. The deposition process took 1 hour, and the body has the following dimensions: diameter of 70 mm, height of 120 mm, number of layers 60.

Figure 8: Square-to-cylinder body

The next stage of the research was to additively manufacture a real functional machine part using the abovementioned process parameters and taking into consideration the peculiarities of printing a square-to-cylinder body.

As a traditional manufacturing process of a compressor impeller is costly and labor-consuming due to its complex geometry, this component was chosen as the next test sample. The scaled-down prototype of a compressor impeller was printed for 40 minutes and presented in Figure 9. It comprises 15 layers and has the following dimensions: diameter of 80 mm, height of 30 mm [21] .

Figure 9: Compressor impeller prototype

IV. Microstructural Analysis

Preparation of the sample (see Figure 10) for micro structural analysis includes the following stages:

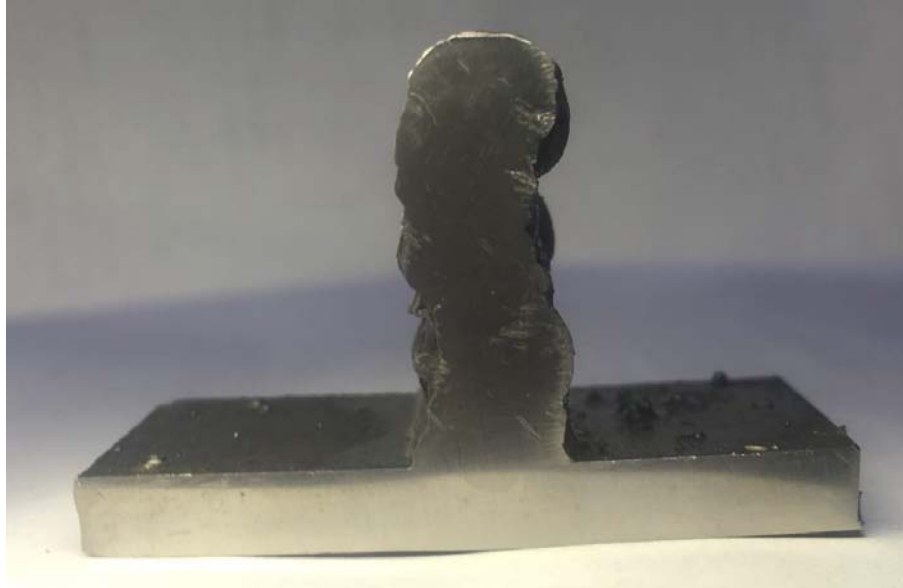- rough grinding;
- final grinding;
- polishing;
- etching.

Figure 10: Sample for microstructural analysis

Rough grinding is performed for the leveling of a surface of the sample using an engineer's file. Then a final grinding follows. Final grinding is performed to minimize surface imperfections using abrasive paper of decreasing grain size. Corundum, carborundum, and other solids are used as abrasives deposited on abrasive papers.

The next stage of preparation is polishing, which is necessary for the final alignment of the surface of the sample. Polishing is carried out using a polishing machine, the working body of which is a rotating disk covered with fabric.

Etching of the polished sample is performed to reveal a complete picture of the microstructure (grain shape and size, presence of phases, structural components). Before etching, the surface of the sample is degreased with alcohol. The sample is etched with Keller's reagent (2 ml HF, 3 ml HCl, and 5 ml HNO3 in 190 ml of water) for 10-20 seconds. After etching, the sample is washed with water and dried with filter paper.

The sample for microstructural analysis can be divided into 3 sectors: lower, middle, and upper (see Figure 11). The lower sector contacts the cold surface of the substrate metal and experiences a certain heat drop. The metal of the middle sector is characterized by a lower temperature difference since the weld beads of this sector are deposited on the preheated metal of the previous beads.
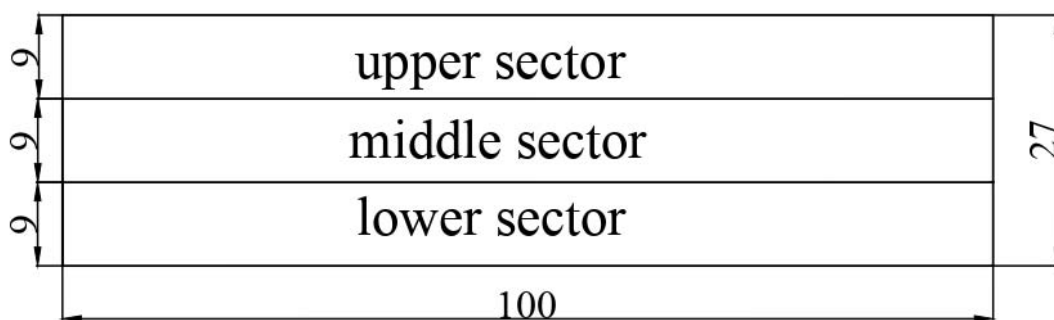

Figure 11: Sectors of the sample

Figure 12 illustrates the microstructure of the lower sector. Equiaxed grains with inclusions of thin lamellas are observed in this sector [19, 20].

Figure 12: The microstructure of the lower sector (ferrite+perlite)

Since the metal is deposited on a cold substrate, the first beads experience a significant temperature difference. This contributes to the formation of a microstructure with ferrite grains and inclusions of lamellar perlite. The formation of ferrite with an equiaxed grain shape with inclusions of lamellar perlite is typical for low-carbon steel, which is the welding wire Sv-08G2S.

Figure 13 illustrates the microstructure of the middle sector. The middle sector is characterized by equiaxed ferrite grains without any inclusions. The microstructure shows that the ferrite of the middle sector has a more coarse-grained structure than in the lower sector. This is due to a higher temperature difference in the lower sector compared with the middle one.

Figure 13: The microstructure of the middle sector (ferrite)

The metal of the middle sector cools slower than that of the upper sector, so its thermal gradient is lower than that in the lower sector. The metal of the lower sector also cools slower than the metal of the upper sector, which results in the formation of ferrite.

The presence of lamellar perlite is explained by a less sharp temperature drop due to the presence of a cold substrate compared with air cooling in the upper sector. Figure 14 illustrates the microstructure of the upper sector.
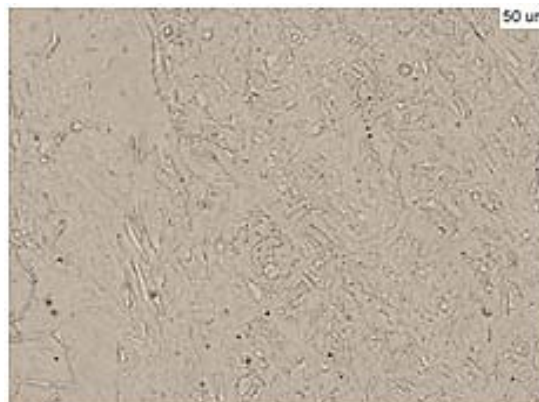

Figure 14: The microstructure of the upper sector (bainite)

As mentioned earlier, it is in this area that a higher temperature drop is observed, so the metal microstructure in this sector is significantly different from others and has a predominantly lamellar structure. In particular, it should be noted that this microstructure is bainite, which is a mixture of ferrite and cementite. Since cooling begins at a temperature of about 70 °C above the critical temperature for the steel used, the growth of ferrite particles devoid of carbon occurs. Since the carbon in ferrite is contained in smaller amounts, it passes to the upper sections and the lamellas are filled with carbon.

It is also worth noting that due to the effect of reheating during the deposition of layers, it is possible to achieve the formation of different microstructures along the height of the sample. This enables adjusting the microstructure between ferrite and bainite to obtain the necessary mechanical properties of the product by alternating cooling cycles after the deposition of one or more layers [22].

V. Hardness Testing

Figure 15 illustrates a diagram with Brinell hardness values. The results obtained show the hardness values in the direction from the lower to the upper sector. The highest values of hardness are observed in the sector with the bainite structure. It is worth noting the almost complete absence of pores, which is a significant advantage in comparison with other additive technologies used for the production of metal products.
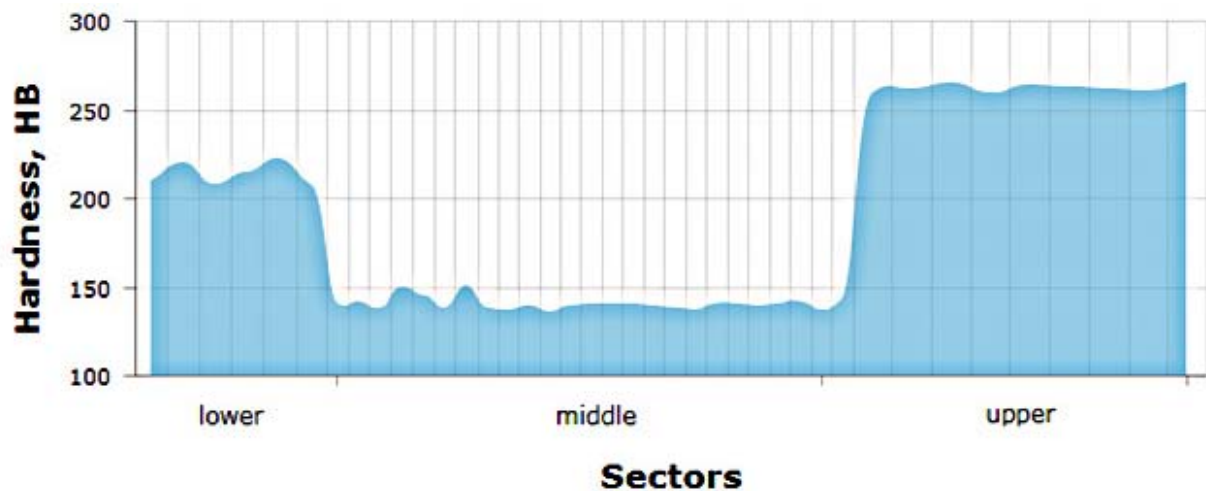

Figure 15: Hardness diagram

The results of hardness measurements confirm the formation of various structures in the sample sectors. Thus, the lower sector, where the structure of ferrite with inclusions of lamellar perlite was formed, has a hardness of 200-220 HB. Higher hardness values of the lower sector compared to the middle sector occur due to inclusions of lamellar perlite.

The middle sector has a purely ferritic structure, which is proved by the lowest hardness values compared with all other sectors. Ferrite is soft and plastic. Ferrite hardness values are in the range of 130-150 HB.

The highest hardness values (260 HB) were found in the upper sector. The bainite structure provides high hardness and strength with high plasticity [22].

AB – elasticity area (350-360 MPa);
BC – yield point area (360-405 MPa);
CD – hardening area (405-577 MPa);
DE – failure area (577-432 MPa).

VI. Tensile Testing

The tensile diagram (see Figure 16) shows the dependence of the elongation of the sample on the longitudinal tensile force.

The diagram has four distinctive areas:

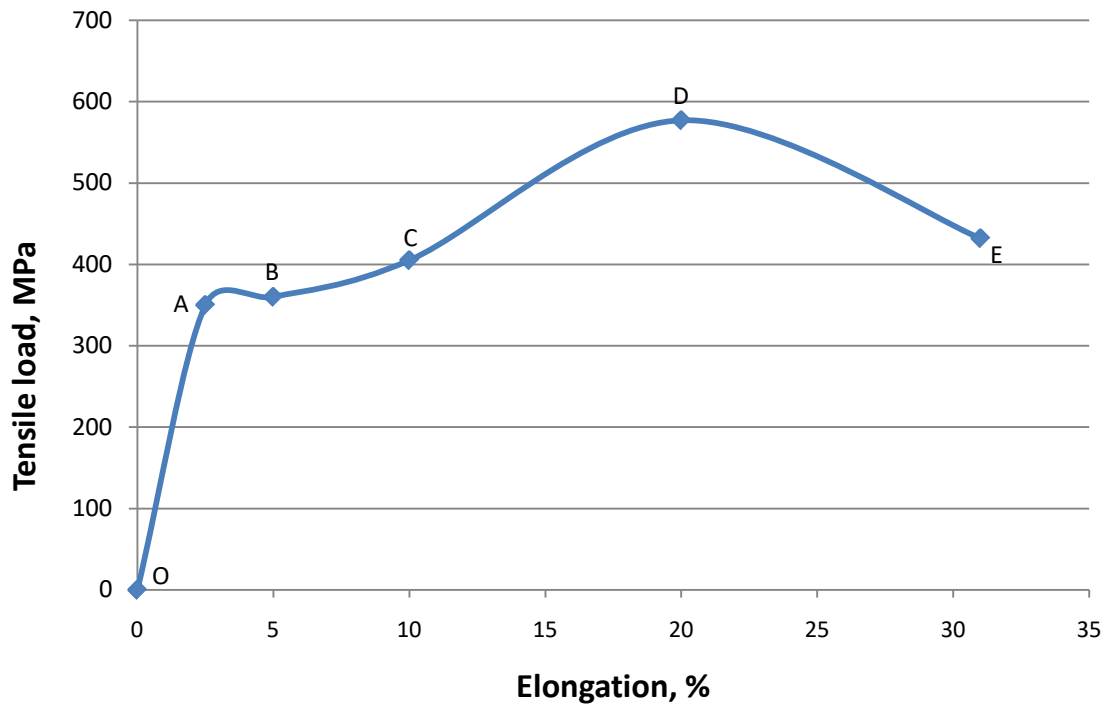OA – proportionality area (0-350 MPa);

Figure 16: Tensile diagram

At the very beginning of the tensile test, the tensile force, and therefore the deformation of the sample, is zero, so the diagram begins at the intersection of the respective axes (point O).

In the OA area, the diagram is drawn as a straight line. This indicates that in this segment of the diagram, the deformations grow in proportion to the increasing load.

Once point A passed, the diagram abruptly changes its direction, and in the AB area the line runs almost parallel to the stretching axis for some time, that is, the deformations increase at almost the same load value.

At this point, irreversible changes begin to occur in the metal of the sample. The crystal lattice of the metal is rebuilt. At the same time, the effect of self-strengthening is observed.

After increasing the strength of the sample material, the diagram goes up again (BC area) and at point D the tensile force reaches the maximum value. At this point, a local thinning appears in the working part of the test sample, caused by violations of the material structure (the formation of voids, microcracks, etc.).

Due to thinning, and therefore reducing the cross-sectional area of the sample, the tensile force required to stretch it is reduced, and the curve of the diagram goes down.

The sample breaks at point E which is the thinning zone.

Mechanical properties of the WAAM Sv-08G2S steel and wrought low carbon steels with comparable chemical compositions are shown in Table 4.

Table 4: Mechanical properties of steels

Steel grade	Test temperature,ºC	YS, MPA	UTS, MPa	Elongation, %	Contraction, %
WAAM Sv-08G2S	20	405	577	31	59
09G2S	20				
09G2T	20	265-385	430-490	17-31	56-63
09G2DT	20				
10G2S1	20	335	485	35	75

As can be seen from the table, the mechanical properties of the wire arc additively manufactured Sv-08G2S steel meet the properties of conventional wrought low-carbon steels and even exceed them [22].

VII. Discussion

In order to improve the stability of the process, eliminate and completely reduce the number of defects in the deposition process, as well as to achieve the accuracy of the deposited parts, it is paramount to determine the correct process parameters. Since a one-time parameter setting is inadequate for obtaining a high-quality part, monitoring and controlling of all parameters is required during the actual deposition process. To do this, appropriate sensors and a video camera with special light filters are needed to be integrated into the existing WAAM complex to remotely monitor and control the process. Moreover, to improve the quality of deposited beads, it is imperative to utilize shielding gases of higher quality. Carbon dioxide alone is not able to provide the necessary quality, so it is preferable to use a mixture of argon and carbon dioxide. To increase the metal deposit factor and hence the WAAM process performance, the wire diameter should be increased from 0.8 to 1-1.2 mm. For the production of real functional parts, it is vital to implement advanced programmable welding machines that allow adjusting the process parameters directly from the robot control interface.

VIII. Conclusions

This article presents the results of the study of the influence of process parameters on the quality of steel components. During the course of the experiment, the relationship between the deposition speed and the geometry of the resulting bead was obtained. The most optimal torch travel speed for the deposition of steel parts using a 0.8 mm wire is 0.003 m/sec at a welding current of 100A. This speed allows achieving the best bead formation with the least distortion. The deposition process itself is quite stable and allows producing beads with approximately the same geometry. At this speed, all layers of the samples are of 2 mm thickness. The most common defects were detected during the deposition of walls, square, and cylindrical samples. Due to the constant and repeated heat input, the geometry of the bead at the beginning and end of the layer is different, which leads to the formation of a slope at the end of the wall. Additionally, there are elements of non-molten wire and splashes of metal. During the deposition of square and cylindrical samples, noticeable defects are unevennesses and widenings at the transition points of the layers, which is caused by the peculiarity of the torch movement. In order to eliminate these defects, it is necessary to develop a path-planning program for more effective planning of the torch movement trajectory. In general, the parameters determined during the experiments can be used for the deposition of real parts prototypes. Further adjustment of the parameters will be required during the actual deposition process to achieve better results.

Based on the results of the study of the microstructure and mechanical properties of the wire arc additively manufactured Sv-08G2S steel, the following conclusions can be drawn:

- The structure of the Sv-08G2S metal can be divided into three sectors depending on the formed microstructure. The lower sector is characterized by a ferritic structure with inclusions of lamellar perlite. The middle sector is characterized by a purely ferritic structure with equiaxed grains. The upper sector is characterized by a lamellar structure of bainite.
- Differences in the microstructure of the sectors are due to various temperature differences and heat input experienced by different deposited beads. In particular, the metal of the upper sector experiences a stronger temperature drop due to the difference in air temperature and the temperature of the lower layers.
- The lower sector is characterized by the presence of smaller particles, so the metal in this sector experiences stronger temperature differences compared to the metal in the middle sector, which is characterized by a larger grain.
- The results of the Brinell hardness study confirm the presence of various microstructures. The hardest was the upper sector, which has a bainite structure.
- The results of tensile testing of samples made of Sv-08G2S steel showed mechanical properties that are comparable and even superior to those of conventional wrought low-carbon steels.

Thus, this steel can be used for wire arc additive manufacturing of steel parts, since the resulting mechanical properties meet the requirements for structural steels.

Also, based on the results of the research, it is possible to develop a technology to obtain the necessary structure of ferrite/bainite in accordance with the requirements for the manufacturing part. Obtaining the necessary microstructure can be achieved by alternating cooling cycles and deposition cycles.

Author Contribution

Anton A. Kulikov performed the experiments, conducted the microstructural analysis, mechanical properties testing, and wrote the paper. Maria V. Grechneva contributed to the microstructure and mechanical properties analysis. Andrei E. Balanovskiy carried out the overall project management and participated in the discussion of the results.

References Références Referencias

1. Wu, B., Pan, Z., Ding, D., Cuiuri, D., Li, H., Xu, J., & Norrish, J. (2018). A review of the wire arc additive manufacturing of metals: properties, defects and quality improvement. Journal of Manufacturing

Processes, 35, 127–139. doi: 10.1016/j.jmapro. 2018.08.001

2. Shi, X., Ma, S., Liu, C., Wu, Q., Lu, J., Liu, Y., & Shi, W. (2017). Selective laser melting-wire arc additive manufacturing hybrid fabrication of Ti-6Al-4V alloy: Microstructure and mechanical properties. Materials Science and Engineering: A, 684, 196–204. https://doi.org/10.1016/j.msea.2016.12.065

3. Horgar, A., Fostervoll, H., Nyhus, B., Ren, X., Eriksson, M., & Akselsen, O. M. (2018). Additive manufacturing using WAAM with AA5183 wire. Journal of Materials Processing Technology, 259, 68–74. https://doi.org/10.1016/j.jmatprotec.2018. 04.014

4. Zhang, C., Li, Y., Gao, M., & Zeng, X. (2018). Wire arc additive manufacturing of Al-6Mg alloy using variable polarity cold metal transfer arc as power source. Materials Science and Engineering: A, 711, 415–423. https://doi.org/10.1016/j.msea.2017.11. 084

5. Wang, J., Pan, Z., Yang, G., Han, J., Chen, X., & Li, H. (2019). Location dependence of microstructure, phase transformation temperature and mechanical properties on Ni-rich NiTi alloy fabricated by wire arc additive manufacturing. Materials Science and Engineering: A, 749, 218–222. https://doi.org/ 10.1016/j.msea.2019.02.029

6. Ding, D., Pan, Z., van Duin, S., Li, H., & Shen, C. (2016). Fabricating Superior NiAl Bronze Components through Wire Arc Additive Manufacturing. Materials, 9(8), 652. https://doi.org/ 10.3390/ma9080652

7. Wu, B., Qiu, Z., Pan, Z., Carpenter, K., Wang, T., Ding, D., Duin, S. V., & Li, H. (2020). Enhanced interface strength in steel-nickel bimetallic component fabricated using wire arc additive manufacturing with interweaving deposition strategy. Journal of Materials Science & Technology, 52, 226–234. https://doi.org/10.1016/j. jmst.2020.04.019

8. Ahsan, M. R. U., Tanvir, A. N. M., Seo, G.-J., Bates, B., Hawkins, W., Lee, C., … Kim, D. B. (2020). Heat-treatment effects on a bimetallic additively-manufactured structure (BAMS) of the low-carbon steel and austenitic-stainless steel. Additive Manufacturing, 32, 101036. https://doi.org/10. 1016/j.addma.2020.101036

9. Williams, S. W., Martina, F., Addison, A. C., Ding, J., Pardal, G., & Colegrove, P. (2016). Wire Arc Additive Manufacturing. Materials Science and Technology, 32(7), 641–647. doi: 10.1179/1743284715y.000000 0073

10. Dickens P, Pridham M, Cobb R, Gibson I, Dixon G. Rapid prototyping using 3-D welding, in. DTIC Document 1992.

11. Spencer J, Dickens P, Wykes C. Rapid prototyping of metal parts by three-di-mensional welding. Proc

Inst Mech Eng Part B J Eng Manuf 1998; 212: 175–82.

12. Kovacevic R, Beardsley H. Process control of 3D welding as a droplet-based Rapid prototyping technique. Proc. Ofthe SFF Symposium, Univ. of Texas at Austin 1998:57–64.

13. Dwivedi R, Kovacevic R. Automated torch path planning using polygon subdivisionfor solid freeform fabrication based on welding. J Manuf Syst 2004;23:278–91.

14. Song YA, Park S, Choi D, Jee H. 3D welding and milling: part I–a direct approach for freeform fabrication of metallic prototypes. Int J Mach Tools Manuf 2005;45:1057–62.

15. Song YA, Park S, Chae S-W. 3D welding and milling: part II—optimization of the 3D welding process using an experimental design approach. Int J Mach Tools Manuf 2005;45:1063–9.

16. Zhang Y, Chen Y, Li P, Male AT. Weld deposition-based rapid prototyping: a pre-liminary study. J Mater Process Technol 2003;135:347–57.

17. Zhang YM, Li P, Chen Y, Male AT. Automated system for welding-based rapid prototyping. Mechatronics 2002;12:37–53.

18. Marenych, O., Kostryzhev, A., Shen, C., Pan, Z., Li, H., & Duin, S. V. (2019). Precipitation Strengthening in Ni–Cu Alloys Fabricated Using Wire Arc Additive Manufacturing Technology. Metals, 9(1), 105. doi: 10.3390/met9010105

19. Donghong Ding, Zengxi Pan, Dominic Cuiuri, Huijun Li, A multi-bead overlapping model for robotic wire and arc additive manufacturing (WAAM) Robot Cim-Int Manuf. 31 (2015) 101-110

20. Filippo Montevecchi, Niccolò Grossi, Hisataka Takagi, Antonio Scippa, Hiroyuki Sasahara, Gianni Campatelli, Cutting Forces Analysis in Additive Manufactured AISI H13 Alloy, Procedia CIRP, Volume 46, 2016, Pages 476-479, ISSN 2212-8271, http://dx.doi.org/10.1016/j.procir.2016.04.034.

21. A A Kulikov et al 2020 IOP Conf. Ser.: Mater. Sci. Eng. 969 012098

22. A A Kulikov et al 2020 IOP Conf. Ser.: Mater. Sci. Eng. 969 012005.